IET Biometrics

Research Article

IET Journals
The Institution of Engineering and Technology

Palm vein recognition scheme based on an adaptive Gabor filter

ISSN 2047-4938
Received on 27th May 2016
Revised 5th December 2016
Accepted on 6th December 2016
E-First on 13th January 2017
doi: 10.1049/iet-bmt.2016.0085
www.ietdl.org

Xin Ma[1] ✉, *Xiaojun Jing*[1], *Hai Huang*[1], *Yuanhao Cui*[1], *Junsheng Mu*[1]

[1]*School of Information and Communication Engineering, Beijing University of Posts and Telecommunications, No. 10, Xitucheng Road, Haidian District, Beijing, People's Republic of China*

✉ *E-mail: xinma@bupt.edu.cn*

Abstract: We propose a novel palm vein recognition scheme based on an adaptive 2D Gabor filter. Three key steps were studied in this scheme: region of interest (ROI) extraction, adaptive Gabor filtering, and template matching. First, in the palm vein image extraction step, the authors used the index finger on both sides of the valley to locate the square area, and then iteratively expanded the area of the square box to maximise the ROI. Second, in the feature extraction step, a novel parameter selection scheme was proposed for optimising the Gabor filter. Third, in the template matching step, the author presented a novel template matching algorithm referred to as the minimum normalised Hamming distance. Experimental results demonstrated that the scheme achieved good performance with an EER of 0.12%.

1 Introduction

In recent years, biometric identification techniques have become an important part of security access systems. Compared to traditional personal identification methods, such as personal identification numbers, magnetic swipe cards, keys, and smart cards, biometric information is harder to observe and can provide a higher security level against identity theft. Among various biometric techniques, palm vein recognition is becoming more popular because it provides invisible internal biometric information and can be measured with a low-cost device.

In this paper, we propose a novel palm vein recognition scheme. This scheme first located the valley on both sides of the index finger in the original image, determines the region of interest (ROI) area of the square, and then iteratively expanded the rectangular ROI to include as much biometric information as possible. The normalized image was then divided into several non-overlapping sub-regions and the optimal parameters of the Gabor filter were determined respectively from each sub-region. The extracted palm vein feature was then encoded into VeinCode [1] format. In the template matching step, the minimum normalized Hamming distance algorithm was applied, which returns the minimum distance value after multiple template displacements. This minimum distance value was used as the final score for template matching.

This paper is organised as follows: Section 2 briefly summarises related work, and Section 3 introduces the process of our proposed method. A novel ROI location method and pre-processing step are described in Section 4. Section 5 introduces a novel Gabor feature extraction algorithm based on an adaptive parameter selection method. Section 6 describes the displacement compensation method for template matching. Experimental results are demonstrated in Section 7, prior to conclusions discussed in Section 8.

2 Related work

The procedure for acquiring palm veins has been described in the literature. Lin [2] investigated palm dorsal images acquired with a thermal infrared device. Subcutaneous blood vessels absorb less radiation than their surroundings in the near-infrared spectrum of 780–1100 nm, resulting in high image contrast. Additionally, Cross [3] investigated hand vein image extraction under near infrared illumination. These studies have been fully described in vein image acquisition literature, but image recognition results obtained using different wavelengths are lacking. Experiments in this area are described in Section 7.5.

Palm vein recognition techniques are divided into four categories. First, geometry-based methods [4, 5] utilise line, curve, and point data to approximate the palm vein. Since these methods require coordinates for precise pattern comparison, the ROI extraction must calibrate position in advance. Second, statistics-based methods [6] use statistical information to recognise pattern features. These can be further divided into global and local static sub-categories. The local static sub-category [7] includes local binary patterns (LBP), local derivative patterns (LDP), Weber local descriptors (WLD), and their variants, and are sensitive to scaling, rotation, and displacement. Previous studies [1, 8] applied Gabor filters to exploit the hand dorsal veins in a spatial domain with good results. On the other hand, the global static sub-category [9] consists of invariant moments, wavelet moments, and gradient fields, and are invariant to scaling, rotation, and displacement. Thirdly, local invariant-based methods [10], such as the scale invariant feature transform (SIFT) and RootSIFT, and square root of SIFT (RootSIFT), extract local invariant palm vein features. However, since features extracted using these methods lack greyscale shift and corners, feature points are small and exhibit many intra-class changes. Fourth, appearance-based methods [11, 12], including principle component analysis (PCA), linear discriminant analysis (LDA), independent component analysis (ICA), and manifold methods acquire palm vein subspace coefficients as features without prior knowledge. This summary of prior work suggests that there is a lack of systematic comparison of different palm vein information processing steps, especially in feature extraction and matching. This has motivated us to further explore palm vein recognition in a more systematic way and to ascertain the best palm vein information processing approach.

3 Overview of proposed scheme

The proposed novel palm vein recognition scheme consists of four basic modules, as shown in Fig. 1. Each of these modules plays a critical role in determining the palm vein matching performance in a biometric recognition system. The functionality of these modules is exhibited as follows:

i. *Pre-processing module*: it determines the ROI position for palm vein images acquired with an NIR illumination device.

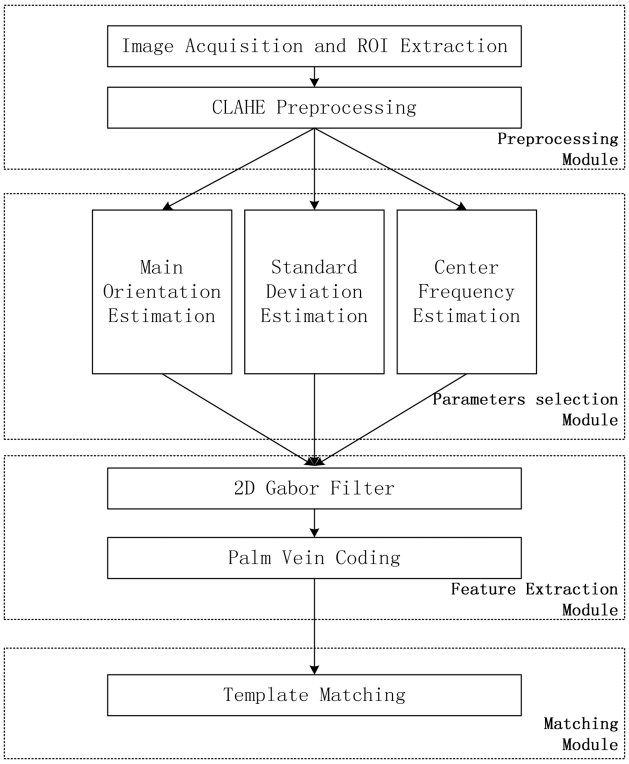

Fig. 1 *Framework of our proposed palm vein recognition system*

ii. *Parameter selection module*: first, it divides the palm vein image into 8×8 non-overlapping sub regions, and estimates the parameters of a 2D Gabor filter containing main orientation, centre frequency, and standard deviation.
iii. *Feature extraction module*: it codes the palm vein feature into VeinCode format, in which the real and imaginary parts of the 2D Gabor result are stored in a binary feature matrix.
iv. *Matching module*: it compares the template with the target pattern using the minimum normalised Hamming distance method, which compensates for ROI calibration errors in the pre-processing step.

4 Image acquisition and enhancement

4.1 Hand shape segmentation and ROI extraction

Segmentation is an important step in separating the palm vein area from the original image. We used the OTSU method to extract hand contours from original greyscale images. The OTSU method, named after Nobuyuki Otsu, is an effective and automatic image thresholding method used for segmentation.

To locate the correct position of an ROI, we located key points on the palm that contained peaks and valley points. Five red points and four green points represent finger tips and finger valleys, respectively.

We defined the tip points P_{t1} through P_{t5} as the fingertips of the thumb, index, middle, ring, and little fingers, respectively. The valley points between those fingers were defined as P_{v1} through P_{v4}.

Several ROI location studies [4, 8, 13] have used P_{v2} and P_{v3} to correctly locate the ROI, but the ROI size was not a maximum. Thus, to enlarge the ROI and accommodate more biometric information, we propose a novel ROI extraction method that can acquire square ROIs as large as necessary.

In (1), d denotes the distance between valley point P_{v1} and P_{v2}, and θ denotes the angle between line segment $\overline{P_{v1}P_{v2}}$ and the vertical, respectively.

$$d = \sqrt{(x_{P_{v1}} - x_{P_{v2}})^2 + (y_{P_{v1}} - y_{P_{v2}})^2} \tag{1}$$

$$\theta = \tan^{-1}\frac{(x_{P_{v1}} - x_{P_{v2}})}{(y_{P_{v1}} - y_{P_{v2}})}. \tag{2}$$

The bilinear grey value differential method was adopted to perform a rotation of θ degrees to ensure the line segment $\overline{P_{v1}P_{v2}}$ was horizontal. Then, the line segment $\overline{P_{v1}P_{v2}}$ was set as an edge of a square ROI box, and P_{v2} was fixed while the ROI was enlarged to the desired size. All elements in the ROI (square matrix) were 1, and therefore we could scale up the square matrix dimensions iteratively until it no longer accommodated additional 1 s. This method also provided maximising ROI size while preventing incorrect palm location. Fig. 2 shows the process of the proposed ROI method.

4.2 Image enhancement

Compared to the image taken in a white light environment, the contrast of the palm vein image captured by the NIR illumination capture device is relatively low. Therefore, direct extraction and feature matching will affect the performance of the biometric recognition system.

Inspired by earlier studies using the CLAHE method for enhancing low-contrast images, this method increases the dynamic range of the image so that palm vein patterns can be more easily detected during feature extraction. As shown in Fig. 3, this method improved contrast between the vein pattern and the background and limited surrounding noise.

For convenience in the feature extraction step, we normalised the ROI size into 256×256 pixels using a bilinear interpolation scale method.

5 Feature extraction

5.1 Overview of 2D adaptive Gabor filter

Gabor filtering is a powerful feature analysis function in computer vision because it is similar to the receptive field profiles in mammalian cortical simple cells. Previous researchers have successfully applied Gabor filters to exploit different biometric characteristics such as faces, irises, fingerprints, and palm prints.

A circular 2D Gabor filter is an oriented complex sinusoidal grating modulated by a 2D Gaussian function as expressed as

$$G_{\sigma,\mu,\theta}(x, y) = g_{\sigma}(x, y) \cdot \exp\{2\pi \mathrm{j}\mu(x\cos\theta + y\sin\theta)\}, \tag{4}$$

where $j = \sqrt{-1}$ and $g_{\sigma}(x, y)$ is a Gaussian envelope defined as

$$g_{\sigma}(x, y) = \frac{1}{2\pi\sigma^2} \cdot \exp\left\{\frac{-(x^2 + y^2)}{2\sigma^2}\right\}. \tag{5}$$

In (5), σ denotes the standard deviation of a Gaussian envelope, μ denotes the frequency of the span-limited sinusoidal grating, and θ denotes the orientation in the interval 0°–180°. Using Euler's formula, the $G_{\sigma,\mu,\theta}(x, y)$ term can be decomposed into a real part, $R_{\sigma,\mu,\theta}(x, y)$, and an imaginary part, $I_{\sigma,\mu,\theta}(x, y)$, as shown in (6)–(8). The real part is suitable for ridge detection in a palm vein image, while the imaginary part is beneficial for edge detection.

$$G_{\sigma,\mu,\theta}(x, y) = R_{\sigma,\mu,\theta}(x, y) + \mathrm{j} \cdot I_{\sigma,\mu,\theta}(x, y) \tag{6}$$

$$R_{\sigma,\mu,\theta}(x, y) = g_{\sigma}(x, y) \cdot \cos[2\pi\mu(x\cos\theta + y\sin\theta)] \tag{7}$$

$$I_{\sigma,\mu,\theta}(x, y) = g_{\sigma}(x, y) \cdot \sin[2\pi\mu(x\cos\theta + y\sin\theta)] \tag{8}$$

However, 2D Gabor filters have a slight response to regions of uniform luminance. This is called direct current (DC) [1]. To make the Gabor filter provide an illumination-insensitive response, we applied (9) to remove the DC component:

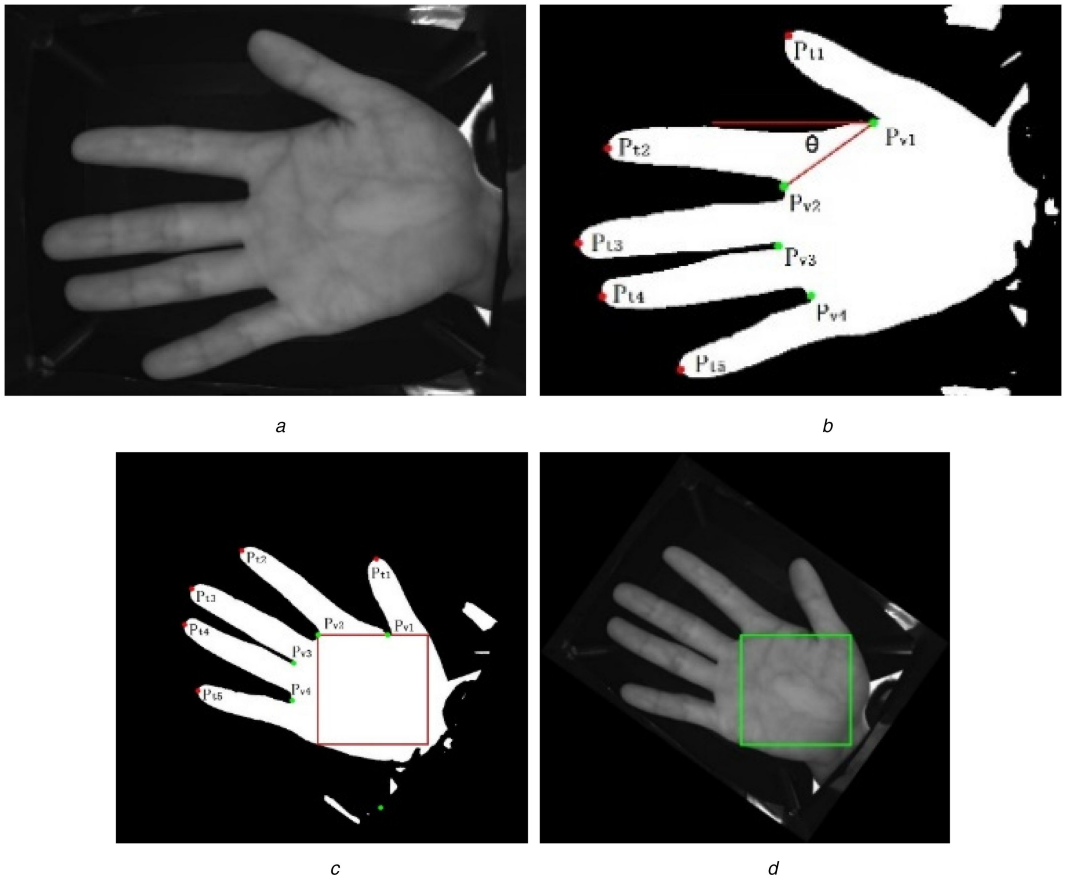

Fig. 2 *Illustration of ROI acquisition and enhancement* ***(a)*** *The original hand image,* ***(b)*** *The key points on the palm,* ***(c)*** *square area of ROI,* ***(d)*** *Final result*

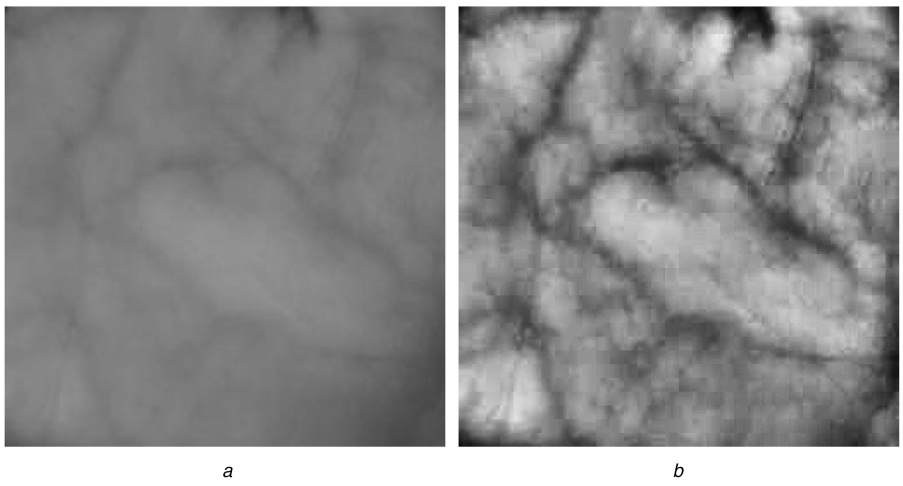

Fig. 3 *Extracted ROI image and the CLAHE result* ***(a)*** *Before CLAHE processing,* ***(b)*** *After CLAHE processing*

$$\tilde{G}_{\sigma,\mu,\theta}(x,y) = G_{\sigma,\mu,\theta}(x,y) - \frac{\sum_{i=-k}^{k}\sum_{j=-k}^{k} G_{\sigma,\mu,\theta}(i,j)}{(2k+1)^2}, \quad (9)$$

where $(2k+1)^2$ is the size of the 2D Gabor filter.

Thus, a Gabor transform with robust illumination is defined in (10), where $I(x,y)$ is a palm vein image and $\otimes$ denotes a convolution operator.

$$F(x,y;\sigma,\mu,\theta) = I(x,y) \otimes \tilde{G}_{\sigma,\mu,\theta}(x,y) \quad (10)$$

Previous research [14] has demonstrated that 2D Gabor filter-based edge detection yields best performance when filter parameters are in line with the direction θ, the variance σ, and the center frequency μ of the input image texture. Based on this idea, this paper proposes segmentation of ROI images into several sub-regions and then determines their optimal Gabor parameter combinations.

In the image acquisition and enhancement step, the ROI size was normalised to 256×256 pixels. We divided the ROI into 8×8 non-overlapping sub-regions to determine the local 2D Gabor parameters independently. Each sub-region was 32×32 pixels. We used the method described in the following section to select the parameters σ, μ, and θ for the 2D Gabor filter in each sub-region.

5.2 Estimation of main orientation

For every palm vein sub-region in the ROI, continuous line-like texture features exhibit a certain tendency in the so-called principal directions. The parameter θ in the 2D Gabor filter represents this orientation and is an intrinsic property of the palm vein. Different from Han's method [15], we adopted a Radon transform-based method rather than 3×3 pixels direction operators. This is because the Radon transform-based method can extract the orientation feature of the palm vein more accurately, especially when vein

texture has not only a local direction feature but also a global direction feature. In contrast, Han's method can only determine the local direction feature because the mask pattern is only 3×3 pixels.

The Radon transform is an effective tool for identifying the structure of continuous lines by integrating intensity along all possible lines in an image. The 2D Radon transform of a given image $h(x, y)$ is defined as follows:

$$\text{Radon}(k, b)[h(x, y)] = \int_{-\infty}^{+\infty} \int_{-\infty}^{+\infty} h(x, y)\delta[y - (kx + b)]\, \mathrm{d}x\, \mathrm{d}y, \tag{11}$$

where k is the slope of the line, and b is the intercept.

According to characteristics of the palm vein image, and based on the Radon transform, Jia [16] proposed the modified finite radon transform (MFRAT), with the definition of $Z_p = \{0, 1, \ldots, p-1\}$, where p is a positive integer. The MFRAT of a real function $f(i, j)$ on the finite grid Z_p^2 is defined as follows:

$$\text{MFART}_f(k) = \sum_{(i,j) \in L_k} f(i, j), \tag{12}$$

where L_k denotes the set of points that comprise a line on the finite grid Z_p^2:

$$L_k = \left\{(i, j) |\ j = k(i - i_0) + j_0, \quad i \in Z_p\right\}. \tag{13}$$

Later, to overcome some shortcomings of MFRAT, Zhou [17] proposed the Gaussian-Radon transform for biometric feature extraction. The Gaussian-Radon transform of a pixel (x_0, y_0) in every sub-region of a palm vein image $I[x, y]$ is defined as

$$\text{GR}_I(k, \sigma_{\text{GR}}; x_0, y_0) = \sum_{(x,y) \in L_k} I[x, y] \times \frac{G_{\text{env}}(x, y)}{\sum_{(x,y) \in L_k} G_{\text{env}}(x, y)}, \tag{14}$$

where (x, y) denotes the neighbourhood of a centre point (x_0, y_0). The $G_{\text{env}}(x, y)$ term is a Gaussian envelope as defined in (15), in which σ_{GR} controls the contribution degree of the neighbourhood points (x, y) to the central point (x_0, y_0).

$$G_{\text{env}}(x, y) = \frac{1}{2\pi\sigma_{\text{GR}}^2} \exp\left\{-\frac{(x - x_0)^2 + (y - y_0)^2}{2\sigma_{\text{GR}}^2}\right\} \tag{15}$$

We used the winner-take-all rule to determine the final direction of the point (x_0, y_0) in Z_p^2:

$$D_k(x_0, y_0) = \underset{k}{\text{argmin}}\left(\text{GR}_I(k, \sigma_{\text{GR}}; x_0, y_0)\right). \tag{16}$$

Considering both computational complexity and verification accuracy, the literature [18] shows that six orientations achieve the best results. Therefore, we selected the optimum direction of a Gaussian-Radon transform of L_k at 0°, 30°, 60°, 90°, 120°, and 150°.

The orientation matrix (OM) was obtained by moving the center point (x_0, y_0) over an entire sub-region pixel by pixel:

$$\text{OM} = \begin{bmatrix} D_k(1,1) & D_k(1,2) & \cdots & D_k(1,n) \\ D_k(2,1) & D_k(2,n) & \cdots & D_k(2,n) \\ \vdots & \vdots & \ddots & \vdots \\ D_k(m,1) & D_k(m,2) & \cdots & D_k(m,n) \end{bmatrix}. \tag{17}$$

Finally, the main orientation θ of a sub-region was determined by statistical distribution of the local orientation in OM:

$$\theta = \arg\max_{\varphi}\left(\sum_{x_0=1}^{n} \sum_{y_0=1}^{m} (D_k(x_0, y_0) = \varphi)\right), \tag{18}$$

where $\varphi \in \{0^\circ, 30^\circ, 60^\circ, 90^\circ, 120^\circ, 150^\circ\}$.

5.3 Estimation of standard deviation

The standard deviation of a Gaussian distribution is represented by σ, which is related to the width of the envelop for modulating a 2D Gabor filter. The Gabor filter is more robust to noise when choosing a large σ value; in this case, the filter will have lost ridge details. In contrast, the Gabor filter will capture more ridge details when using a small σ value, but the convolution result will be affected by noise. In Han's method [15], the standard deviation is an empirical value from the training samples, and therefore, it cannot ensure good generalisation in test data. In our algorithm, we determined the standard deviation of Gabor filter σ by measuring the local region variance of the image $D(I(i, j))$.

More concretely, we chose a different σ value by measuring the degree of ridge detail in all sub-regions. Equations (19) and (20) express the image deviation for a local region where σ is predefined as some fixed value according to changes in image texture detail:

$$E(I(i, j)) = \frac{\sum_{i=1}^{m} \sum_{j=1}^{n} I(i, j)}{m \times n}, \tag{19}$$

$$D(I(i, j)) = \sqrt{\frac{\sum_{i=1}^{m} \sum_{j=1}^{n} (I(i, j) - E(I(i, j)))^2}{m \times n}}, \tag{20}$$

where $E(I(i, j))$ denotes the mean value of a sub-region, and $D(I(i, j))$ denotes the image deviation in a sub-region.

For the palm vein image, after the CLAHE pre-processing step, the term $\sigma \in \{1, \sqrt{2}, 2\sqrt{2}, 4\sqrt{2}\}$ is optimal, as is in (21):

$$\sigma = \begin{cases} 1, & \text{if } D(I(i, j)) \le 1 \\ \sqrt{2}, & \text{if } 1 < D(I(i, j)) \le 1.4 \\ 2\sqrt{2}, & \text{if } 1.4 < D(I(i, j)) \le 2.8 \\ 4\sqrt{2}, & \text{if } D(I(i, j)) > 2.8 \end{cases}. \tag{21}$$

These values indicate a stable area, a slowly changing area, a moderately changing area, and a drastically changing area, respectively.

5.4 Estimation of center frequency

In general, changing grey levels in the main direction are seen as a sine wave. The distance T between two ridges or two edges can be calculated, and the center frequency μ can be measured by $\mu = 1/T$. However, this method is not sufficient for palm vein recognition systems due to the fact that the pattern is too blurry to distinguish between ridges and edges.

Previous experiments have shown that the Gabor filter is not sensitive to the center frequency [15]. Therefore, we divided all center frequencies into four range groups and specified a fixed frequency value using the standard deviation σ, which was determined in a previous step.

After careful observation, we recognised that sub-regions in the palm vein image contained complex feature texture (high σ value) when the T value was small, and vice versa. Therefore, we estimated the center frequency μ using the standard deviation value σ directly:

$$\mu = \begin{cases} 0, & \text{if } \sigma = 1 \\ 0.12, & \text{if } \sigma = \sqrt{2} \\ 0.8, & \text{if } \sigma = 2\sqrt{2} \\ 2, & \text{if } \sigma = 4\sqrt{2} \end{cases}. \tag{22}$$

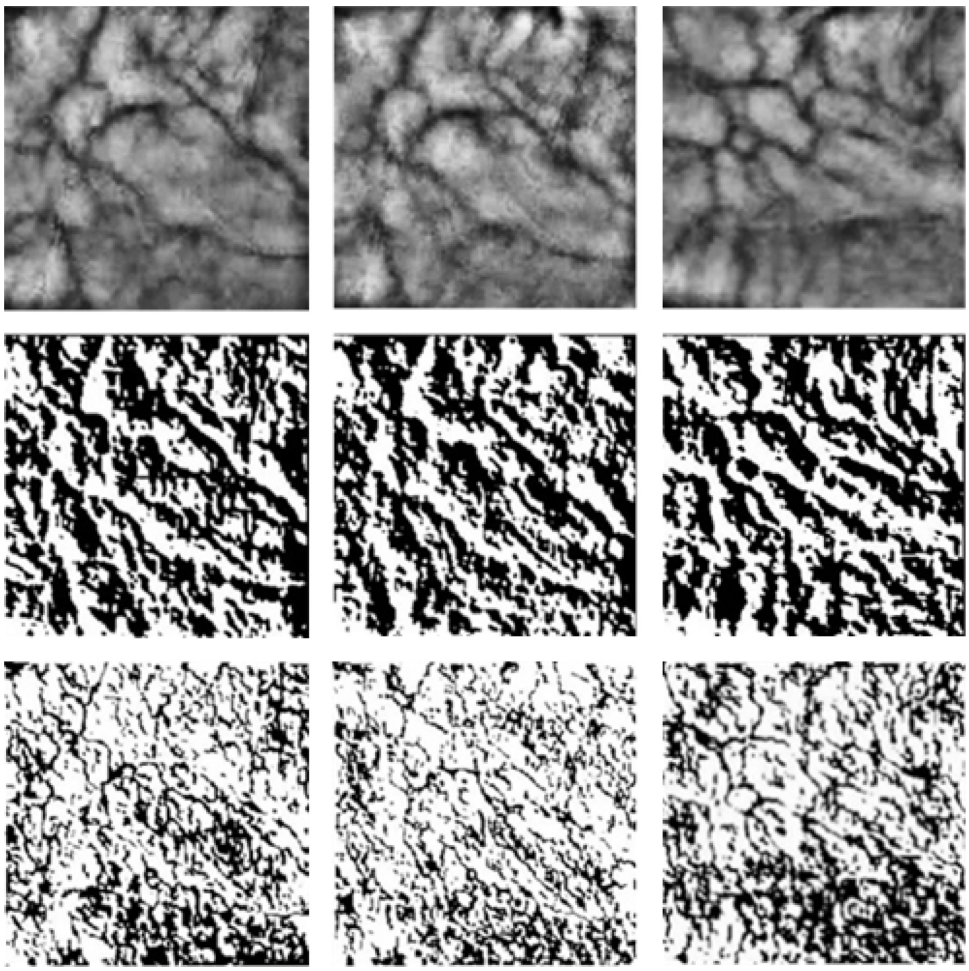

Fig. 4 *Real and imaginary parts in VeinCode feature matrix. The left and middle columns show features from the same person, while the right column shows features from a different person*

Using (22) to estimate the center frequency enhanced the operational efficiency because the computational cost of insensitive parameters in the Gabor filter was reduced.

5.5 Palm vein feature coding

According to the above methods, we independently estimated the σ, μ, and θ parameters for a 2D Gabor filter for every sub-region. For a neighborhood window of size $S \times S$, with $S = 2K + 1$, the real part of the image, $\mathrm{CR}_{\sigma,\mu,\theta}(x, y)$, and the imaginary part of the image, $\mathrm{CI}_{\sigma,\mu,\theta}(x, y)$, in the 2D Gabor filter were calculated by discrete convolution. Each sub-region was convolved with a 2D Gabor filter until the whole ROI image was traversed:

$$\mathrm{CR}_{\sigma,\mu,\theta}(x, y) = \sum_{i=-k}^{k} \sum_{j=-k}^{k} I(x + i, y + j) \cdot R_{\sigma,\mu,\theta}(x, y) \tag{23}$$

$$\mathrm{CI}_{\sigma,\mu,\theta}(x, y) = \sum_{i=-k}^{k} \sum_{j=-k}^{k} I(x + i, y + j) \cdot I_{\sigma,\mu,\theta}(x, y) \tag{24}$$

Finally, features extracted from the palm vein image were encoded into a binary form $(V_{\mathrm{R}}, V_{\mathrm{I}})$, i.e. the VeinCode, as defined in (25) and (26), respectively:

$$V_{\mathrm{R}}(x, y) = \begin{cases} 1, & \text{if } \mathrm{CR}_{\sigma,\mu,\theta}(x, y) \geq 0 \\ 0, & \text{if } \mathrm{CR}_{\sigma,\mu,\theta}(x, y) < 0 \end{cases}, \tag{25}$$

$$V_{\mathrm{I}}(x, y) = \begin{cases} 1, & \text{if } \mathrm{CI}_{\sigma,\mu,\theta}(x, y) \geq 0 \\ 0, & \text{if } \mathrm{CI}_{\sigma,\mu,\theta}(x, y) < 0 \end{cases}. \tag{26}$$

In Fig. 4, the left and middle columns show the real and imaginary parts in the VeinCode feature matrix for the same person acquired over time. In contrast, the right column shows the VeinCode feature matrix for a different person. These images show that the features from the same person are obviously similar, while those from a different person are very different. This suggests that the resulting 2D Gabor filter can be used as an identification feature.

6 Template matching

6.1 Displacement compensation

Since ROI calibration on a palm vein image will inevitably lead to some degree of displacement deviation, which will affect the final performance of a recognition system, it is necessary to compensate for this displacement deviation. A similar approach to compensate for the displacement deviation was proposed by Kang [13], which compared the ratio of the number of matching pixels with the total number of pixels. In our algorithm, we compared multiple palm vein images using the NHD method (discussed in the next section), which was iteratively derived by shifting along the horizontal and vertical directions. We regarded the minimum distance scalar value among all possible displacement as the final comparison result. Thus, displacement compensation was then completed. This method was more robust than Kang's method because the NHD method itself provides slight translation and rotation invariance characteristics.

By keeping the template palm vein image fixed and moving the target palm vein image along the horizontal and vertical directions, the overlapping region was utilised for pattern matching. Since the ROI images were 256×256 pixels, the possible region was 248×248 pixels when setting the threshold at 8 pixels. Possible offset cases typically occurred with respect to the template image (I_1) and target image (I_2), as shown in Fig. 5.

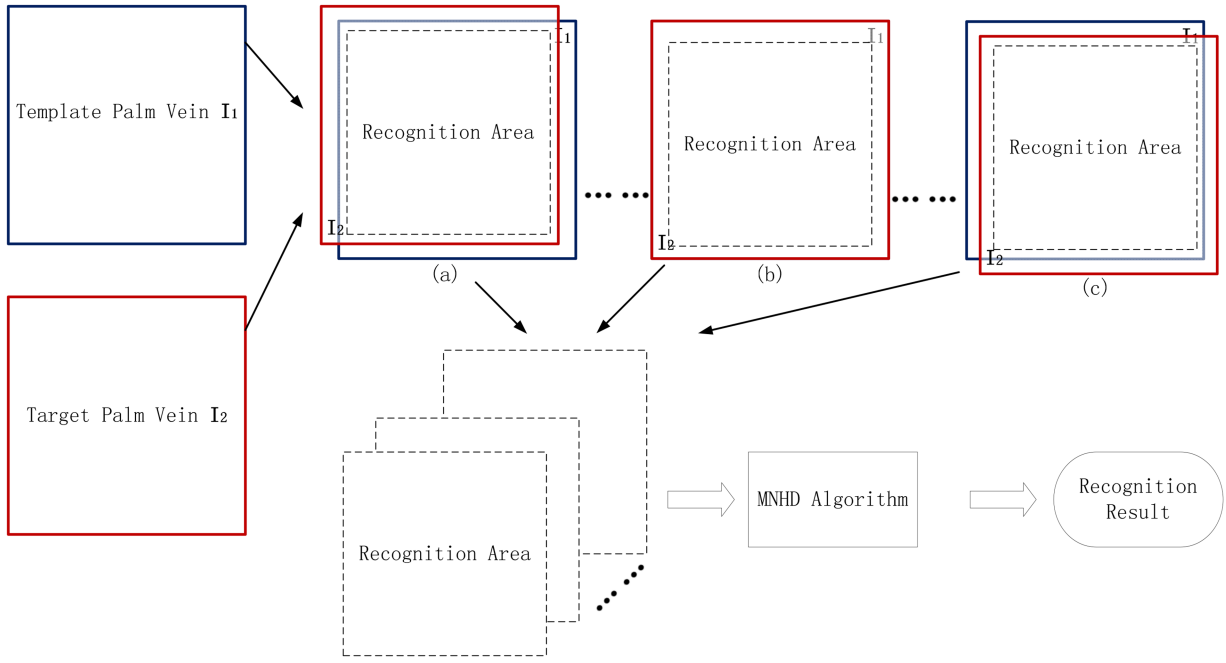

Fig. 5 *Illustrations of four possible overlapping recognition areas*

After this step, we obtained a set of recognition regions, which were then used to calculate similarity by the minimum normalized Hamming distance (MNHD) algorithm. This algorithm is discussed in the next section.

6.2 Minimum normalised Hamming distance

Based on Lee's normalised Hamming distance (NHD) method [1], we propose the minimum normalised Hamming distance (MNHD) algorithm, which considers the displacement compensation problem presented in the previous section, and thus extends the application of Lee's method.

Since palm vein features are encoded into a binary VeinCode matrix using (25) and (26), the Normalised Hamming distance (NHD) was adopted to determine the similarity between a template and target palm vein features. Furthermore, the NHD provides slight translation and rotation invariance matching, which is necessary for palm vein identification systems. The definition of the NHD is as follows: (see (27)) In (27), P and Q are the template and target palm veins, respectively; P_{R} and Q_{R} represent the real parts after Gabor convolution; P_{I} and Q_{I} represent the imaginary parts after Gabor convolution; $\otimes$ denotes a Boolean XOR operator; the size of the feature matrix is $N \times N$; S and T denote the maximum allowable offset in the horizontal and vertical directions, respectively, and $H(x) = \min(N, N + x) - \max(1, 1 + x)$.

Additionally, NHD values ranged from 0 to 1. Thus, if a template and a target palm vein feature matrix matched perfectly, the NHD value was 0.

By calculating the feature distance among all possible displacement deviations along the horizontal and vertical directions, the minimum distance value was regarded as the final matching score. This MNHD method can solve the problem of displacement deviation while calibrating the ROI step, thereby improving accuracy of the palm vein recognition system.

In implementation, template matching is affected by different offsets along the horizontal direction (α pixels) and the vertical direction (β pixels). Using (27), we calculated the distance value $\mathrm{NHD}(\alpha, \beta)$ at all possible deviation positions in (28), and filled a displacement distance matrix (***DDM***):

$$\boldsymbol{DDM} = \begin{bmatrix} \mathrm{NHD}(1,1) & \mathrm{NHD}(1,2) & \cdots & \mathrm{NHD}(1,\beta) \\ \mathrm{NHD}(2,1) & \mathrm{NHD}(2,n) & \cdots & \mathrm{NHD}(2,\beta) \\ \vdots & \vdots & \ddots & \vdots \\ \mathrm{NHD}(\alpha,1) & \mathrm{NHD}(\alpha,2) & \cdots & \mathrm{NHD}(\alpha,\beta) \end{bmatrix}. \quad (28)$$

In our palm vein recognition system, the threshold of maximum displacement compensation was 8 pixels, and thus the displacement distance matrix was 8×8.

The algorithm for MNHD matching is as follows (Fig. 6):

7 Experimental results

7.1 Database

Evaluation experiments were conducted on the CASIA-MS-PalmprintV1 database [19] (CASIA database). The CASIA database contains 7200 palm images acquired using a non-contact device. All images were captured from 100 different people and each sample contains six palm images at different wavelengths of light (460, 630, 700, 850, and 940 nm).

We selected the 940 nm wavelength group. Furthermore, to increase the number of inter-class sample comparisons, we regarded the left hand and right hand samples as being from different people. As a result, there were 200 different people in this experimental database and each sample contained six palm vein images.

7.2 Performance evaluation of proposed method

Discriminating power matching experiments were conducted between genuine and imposter groups that included intra- and inter-class matches. Intra-class matching is defined as matching between a sample and other samples in the same class, whereas inter-class matching is defined as matching between a sample and other samples belonging to a different class.

We adopted the minimum normalised Hamming distance to evaluate our proposed method. Fig. 7 shows a histogram of the distance for genuine and imposter palm vein samples. The left line shows a distribution for intra-class matching, while the right line shows a distribution for inter-class matching. The distribution of intra-class was significantly lower than inter-class, which implies

$$\mathrm{NHD} = \frac{\sum_{i=\max(1,1+S)}^{\min(N,N+S)} \sum_{j=\max(1,1+T)}^{\min(N,N+T)} \left[P_{\mathrm{R}}(i+S, j+T) \otimes Q_{\mathrm{R}}(i,j) + P_{\mathrm{I}}(i+S, j+T) \otimes Q_{\mathrm{I}}(i,j) \right]}{2H(S)H(T)}. \quad (27)$$

Algorithm: MNHD matching

01. //Input
02. F_{target} //target feature matrix
03. $F_{template}$ //template feature matrix
04. $D_{\text{deviation}}$ //displacement deviation pixels
05. //Output
06. R_{Result} // 1 for accept, 0 for reject
07. //Initialize
08. matrix ***DDM*** //has $(2D_{\text{deviation}}+1)^2$ dimensions
09. //Begin algorithm
10. **FOR** $\alpha = -D_{\text{deviation}}$ TO $D_{\text{deviation}}$ {
11. **FOR** $\beta = -D_{\text{deviation}}$ TO $D_{\text{deviation}}$ {
12. Get the recognition area from overlapped region between target and template feature matrix.
13. Calculate the NHD using Eq. (27).
14. Save current NHD(α, β) value to matrix ***DDM***.
15. }
16. }
17. **IF** **Min**$\{all\ elements\ in\ \boldsymbol{DDM}\} \le T_{threshold}$
18. RETURN $R_{Result} = 1$ //accept
19. **ELSE**
20. RETURN $R_{Result} = 0$ //reject
21. //End algorithm

Fig. 6 *Algorithm: MNHD matching*

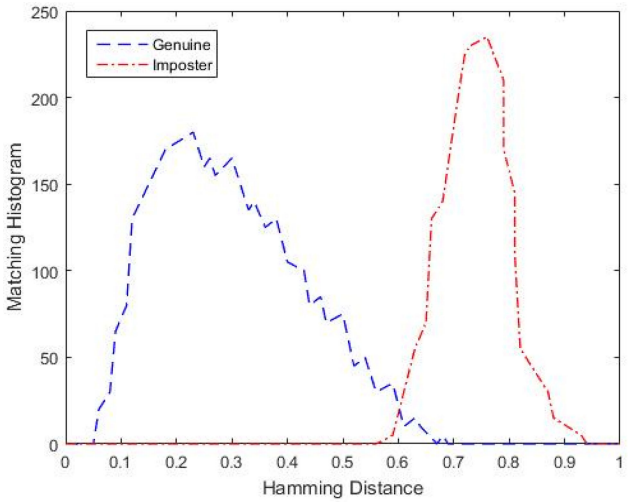

Fig. 7 *Hamming distance measurement histogram*

the normalised Hamming distance of VeinCode features for the same person was significantly lower than the matching score for different people. The intersection of the two curves, the distance axis at 0.6, is a reasonable threshold for discrimination.

We evaluated the equal error rate (EER) of our proposed method by making trade-offs between the false rejection rate (FRR) and the false acceptance rate (FAR). This is shown in the receiver operating characteristic curve (ROC) where the EER of our proposed method was 0.12%.

To confirm the robustness of the displacement compensation scheme in the matching step, we evaluated recognition performance using the proposed palm vein recognition method based on two types of matching schemes: with displacement compensation and without displacement compensation.

We used the ROC curves to analyse the recognition performance of these two experiments. Fig. 8 shows the FAR and FRR distributions for the two matching schemes. The entire curve with displacement compensation was located below the curve without displacement compensation. Experimental results show that the displacement compensation method improved recognition performance and reduced EER by up to 0.1%.

To evaluate the optimisation parameters of Gabor filter standard deviation σ and center frequency μ, we experimented with a variety of combinations of parameters. First, we divided the image deviation into 4 intervals, i.e. $A \in (0, 1]$, $B \in (1, 1.4]$, $C \in (1.4, 2.8]$, and $D \in (2.8, +\infty)$, and evaluated the effect of different standard deviation combinations $(\sigma_A, \sigma_B, \sigma_C, \sigma_D)$ from different intervals. Then, when the value of the standard deviation was fixed, we selected the optimal frequency parameter combination $(\mu_A, \mu_B, \mu_C, \mu_D)$ in a similar way. Table 1 illustrates the evaluation result. When $(\sigma_A, \sigma_B, \sigma_C, \sigma_D) = (1, \sqrt{2}, 2\sqrt{2}, 4\sqrt{2})$ and $(\mu_A, \mu_B, \mu_C, \mu_D) = (0.00, 0.12, 0.80, 2.00)$, performance of the recognition system was optimal (bold in Table 1). Therefore, we selected these parameter combinations for our algorithm, as shown in (21) and (22).

7.3 Comparison and discussion

To further demonstrate the effectiveness of the proposed method, we conducted detailed comparisons with existing conventional methods. To run the algorithms of these conventional methods, we wrote codes based on the corresponding publications. Table 2 illustrates that the EER of our proposed method was 0.12%, which is slightly better than other methods.

The minutiae feature and Hessian phase methods extract locations and local statistical information such as minutiae points

and ridge bifurcations for palm vein texture. However, when texture is unclear or indistinguishable, these methods fail to extract geometric feature information. In contrast, the Laplacian palm method extracts features using LPP and aims to preserve the local structure of the image space, while the eigenvein method extracts features using (2D)2 PCA and aims to preserve the global structure of the image space. The performance of both the Laplacian palm and eigenvein methods was lower than our method. We speculate that this is because these methods do not focus on extracting and matching local palm vein texture information and, as a result, do not have a strong mechanism to accommodate potentially large variations in palm vein patterns.

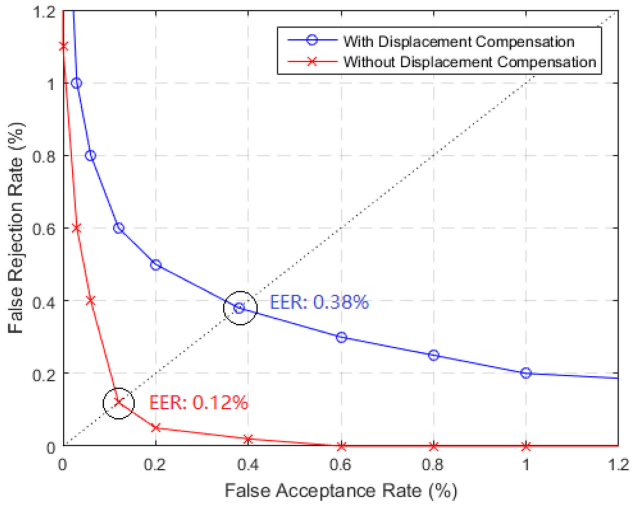

Fig. 8 *ROC curves for two kinds of matching schemes*

7.4 Effects of different ROI methods

Compared with biometric information such as fingerprints, irises, and faces, there are few types of texture patterns, and therefore, the ROI has a direct impact on system recognition rate. We performed experiments to evaluate the effect of different ROI extraction methods on system performance. As shown in Table 3, the selection of an appropriate ROI is critical for achieving higher performance. If the ROI size is too small, it may contain a lower feature pattern and a higher proportion of noise, and therefore making performance suffer.

Comparing Kang and Zhang's method with our ROI extraction method, we concluded that an increasing ROI size improved performance of our recognition scheme. A reasonable explanation is that a larger ROI size can provide more detailed biometric information after normalising the image size, hence improving the accuracy of predicted parameters for the 2D Gabor filter.

The ROI size and sub-region segmentation method are important in our palm vein recognition scheme. To evaluate the performance of our algorithm comprehensively, we conducted a thorough test of these parameters. As shown in Fig. 9, when the ROI size was 256×256, and the number of blocks was 8×8, the performance of our scheme was optimal. These results are consistent with the notion that high-resolution images can provide rich palm vein texture details, which increasing recognition information for our system. Furthermore, in a sub-region too small, palm vein structure information may be lost, while too large of a sub-region may render the adaptive Gabor filter unable to optimise the local parameters.

7.5 Computational efficiency

Finally, we conducted experiments to compare time-consumption of different methods. These experiments were conducted using MATLAB 8.6 on a Windows 64-bit system with an Intel i5-4690 CPU with 8 GB RAM. Repeated random sampling validation was

Table 1 Performance evaluation of parameters combination

$(\mu_A, \mu_B, \mu_C, \mu_D)$	$(\sigma_A, \sigma_B, \sigma_C, \sigma_D)$				
	$(1, \sqrt{2}, 2, 2\sqrt{2})$, %	$(1, \sqrt{2}, 2\sqrt{2}, 3\sqrt{2})$, %	$(1, \sqrt{2}, 2\sqrt{2}, 4\sqrt{2})$, %	$(2, \sqrt{3}, 2\sqrt{3}, 4\sqrt{3})$, %	$(2, 2\sqrt{3}, 4\sqrt{3}, 6\sqrt{3})$, %
(0.00, 0.06, 0.12, 0.24)	7.90	5.61	2.99	6.91	9.66
(0.00, 0.10, 0.20, 0.40)	5.29	3.55	1.74	4.10	7.07
(0.02, 0.08, 0.16, 0.64)	3.93	2.10	0.79	3.58	6.98
(0.50, 0.90, 1.30, 1.50)	3.09	1.44	0.35	2.41	4.55
(0.00, 0.12, 0.80, 2.00)	0.56	0.18	**0.12**	0.96	2.01
(0.30, 0.60, 1.80, 3.60)	1.19	0.87	0.21	1.42	3.55
(1.00, 3.00, 5.00, 7.00)	5.91	3.09	1.47	5.69	9.08

Table 2 Performance comparison of different methods

Methods for palm vein recognition	Year of creation	Performance (EER), %
Laplacian Palm [20]	2007	2.87
Minutiae Feature [21]	2008	2.00
Hessian Phase [4]	2011	1.10
Gabor Filter [15]	2012	0.86
Eigenvein [22]	2008	1.41
local invariant feature [10]	2014	0.99
mutual foreground LBP [13]	2014	0.26
multi-sampling feature fusion [23]	2015	0.16
proposed method		0.12

Table 3 Effects of different ROI methods on the proposed system

ROI extraction method	Mean pixels of ROI	EER, %
Kang's method [13]	44,100 (210 × 210 pixels)	2.22
Zhang's method [24]	22,500 (150 × 150 pixels)	3.15
proposed method	62,500 (250 × 250 pixels)	0.12

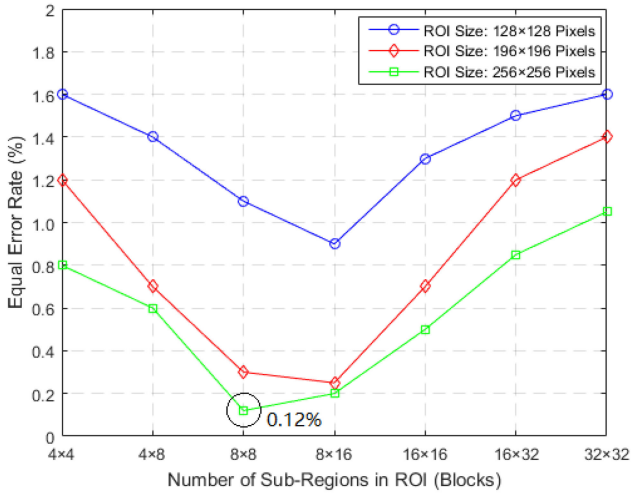

Fig. 9 *Illustrations of EER curve for different ROI and segmentation methods*

Table 4 Operational efficiency of different algorithms

Key steps	Feature extraction, s	Feature matching, s	SUM, s
Laplacian palm [20]	1.36	0.70	2.06
Minutiae feature [21]	7.21	1.21	8.42
Hessian phase [4]	3.38	0.91	4.29
Gabor filter [15]	1.64	1.59	3.23
Eigenvein [22]	1.52	0.62	2.14
local invariant feature [10]	2.55	1.97	4.52
mutual foreground LBP [13]	2.44	2.14	4.58
multi-sampling feature fusion [23]	1.43	1.82	3.25
proposed method	1.28	1.16	2.44

applied to assess computational efficiency, and the results were averaged over 200 iterations.

Our proposed method was more competitive by comprehensive comparison, as shown in Table 4. Experimental results showed that our proposed method required 1.28 s of computation time for the feature extraction step, and was the most efficient of all methods. In the feature matching step, our proposed method required 1.16 s. Although the template matching step in our proposed scheme required additional time, from a systems point of view, the total time consumption for our method was only 2.44 s, which still met practical application requirements.

We analysed the time complexity of the proposed algorithm. For the core code of the feature extraction steps, the 'estimation of main orientation' function must perform an operation in each direction, and therefore the time complexity is $O(n)$. For the core code of feature matching steps, the 'Displacement Compensation' function must iteratively call (27) up to $(2D_{\text{deviation}}+1)^2$ times. Therefore, the time complexity is $O(n^2)$, which illustrates greater computation time requirements.

In our feature matching algorithm, it was possible that more time was spent on the iterative method of calling the MNHD method. We seriously considered the possibility of improving our algorithm, and think that in the future, we can introduce parallel computing technology to speed up feature matching. Therefore, in future studies, we could reduce computation time by optimising the program code.

8 Conclusion

We proposed a reliable and robust palm vein recognition scheme based on an adaptive Gabor filter. A simple but efficient ROI location method was proposed to acquire square ROIs designed to be as large as possible to obtain maximal biometric information. A novel adaptive Gabor filter parameter estimation approach was also presented. The innovative aspects of this approach are as follows: we used the Radon method to determine the local Gabor direction parameter, the degree of image change to determine the local Gabor variance parameter, and the insensitivity of the local Gabor filter to determine its central frequency parameter. Then, to compensate for displacement error in previous ROI steps and further improve feature matching accuracy, we proposed using the NHD to calculate difference values for all possible position displacements. Experimental results show that our scheme achieved good performance with an EER of 0.12%. This performance was superior to other conventional palm vein recognition methods.

9 Acknowledgments

We sincerely thank the Chinese Academy of Sciences' Institute of Automation for providing the CASIA-MS-PalmprintV1 database used in this research.

10 References

[1] Lee, J.C., Lee, C.H., Hsu, C.B., *et al.*: 'Dorsal hand vein recognition based on 2D Gabor filters', *Imaging Sci. J.*, 2014, **62**, (3), pp. 127–138

[2] Lin, C.L., Fan, K.C.: 'Biometric verification using thermal images of palm-dorsa vein patterns', *IEEE Trans. Circuits Syst. Video Technol.*, 2004, **14**, (2), pp. 199–213

[3] Cross, J.M., Smith, C.L.: 'Thermographic imaging of the subcutaneous vascular network of the back of the hand for biometric identification'. Int. Carnahan Conf. on Security Technology, Sanderstead, UK, October 1995, pp. 20–35

[4] Zhou, Y., Kumar, A.: 'Human identification using palm-vein images', *IEEE Trans. Inf. Forensics Sec.*, 2011, **6**, (4), pp. 1259–1274

[5] Song, W., Kim, T., Kim, H.C., *et al.*: 'A finger-vein verification system using mean curvature', *Pattern Recognit. Lett.*, 2011, **32**, (11), pp. 1541–1547

[6] Mirmohamadsadeghi, L., Drygajlo, A.: 'Palm vein recognition with local binary patterns and local derivative patterns'. Int. Joint Conf. on Biometrics, Washington, USA, October 2011, pp. 1–6

[7] Chen, J., Shan, S., He, C., *et al.*: 'WLD: a robust local image descriptor', *IEEE Trans. Pattern Anal. Mach. Intell.*, 2009, **32**, (9), pp. 1705–1720

[8] Lee, J.-C.: 'A novel biometric system based on palm vein image', *Pattern Recognit. Lett.*, 2012, **33**, (12), pp. 1520–1528

[9] Li, X., Guo, S., Gao, F., *et al.*: 'Vein pattern recognitions by moment invariants'. Int. Conf. on Bioinformatics & Biomedical Engineering, Wuhan, China, July 2007, pp. 612–615

[10] Kang, W.X., Liu, Y., Wu, Q.X., *et al.*: 'Contact-free palm-vein recognition based on local invariant features', *PLoS One*, 2014, **9**, (5), pp. 1239–1245

[11] Liu, Z., Yin, Y., Wang, H., *et al.*: 'Finger vein recognition with manifold learning', *J. Netw. Comput. Appl.*, 2010, **33**, (3), pp. 275–282

[12] Yang, G., Xi, X., Yin, Y.: 'Finger vein recognition based on (2D)(2) PCA and metric learning', *J. Biomed. Biotechnol.*, 2012, **2012**, (3), p. 324249

[13] Kang, W.X., Wu, Q.X.: 'Contactless palm vein recognition using a mutual foreground-based local binary pattern', *IEEE Trans. Inf. Forensics Sec.*, 2014, **9**, (11), pp. 1974–1985

[14] Mehrotra, R., Namuduri, K.R., Ranganathan, N.: 'Gabor filter-based edge detection', *Pattern Recogn.*, 1992, **25**, (12), pp. 1479–1494

[15] Han, W.Y., Lee, J.C.: 'Palm vein recognition using adaptive Gabor filter', *Expert Syst. Appl.*, 2012, **39**, (18), pp. 13225–13234

[16] Jia, W., Huang, D.-S., Zhang, D.: 'Palmprint verification based on robust line orientation code', *Pattern Recogn.*, 2008, **41**, (5), pp. 1504–1513

[17] Zhou, Y.J., Liu, Y.Q., Feng, Q.J., *et al.*: 'Palm-vein classification based on principal orientation features', *PLoS One*, 2014, **9**, (11), p. 12

[18] Yue, F., Zuo, W., Zhang, D., *et al.*: 'Orientation selection using modified FCM for competitive code-based palmprint recognition', *Pattern Recogn.*, 2009, **42**, (11), pp. 2841–2849

[19] 'CASIA-MS-PalmprintV1', http://biometrics.idealtest.org/, accessed 20 January 2016

[20] Wang, J.-G., Yau, W.-Y., Suwandy, A., *et al.*: 'Fusion of palmprint and palm vein images for person recognition based on 'Laplacianpalm' feature'. 2007 IEEE Conf. on Computer Vision and Pattern Recognition, Minneapolis, USA, June 2007, pp. 1–8

[21] Wang, L., Leedham, G., Siu-Yeung Cho, D.: 'Minutiae feature analysis for infrared hand vein pattern biometrics', *Pattern Recogn.*, 2008, **41**, (3), pp. 920–929

[22] Wang, J.-G., Yau, W.-Y., Suwandy, A., *et al.*: 'Person recognition by fusing palmprint and palm vein images based on 'Laplacianpalm' representation', *Pattern Recogn.*, 2008, **41**, (5), pp. 1514–1527

[23] Yan, X.K., Kang, W.X., Deng, F.Q., *et al.*: 'Palm vein recognition based on multi-sampling and feature-level fusion', *Neurocomputing*, 2015, **151**, (151), pp. 798–807

[24] Zhang, D., Guo, Z., Lu, G., *et al.*: 'Online joint palmprint and palmvein verification', *Expert Syst. Appl.*, 2011, **38**, (3), pp. 2621–2631